Journal Name

ARTICLE

pH-Triggered Adjustable Bursting of Liquid Marbles on Water Pool

Saurav Kumar,[a] Nishanta Barman,[a] Angana Borbora,[a] Priyam Mondal,[b] Mizuki Tenjimbayashi [d] and Uttam Manna [a,b,c]**

Received 00th January 20xx,
Accepted 00th January 20xx

DOI: 10.1039/x0xx00000x

www.rsc.org/

Non-sticking millimetric droplets wrapped with micron/submicron-sized liquid repellent solid particles and aggregates are recognized as liquid marbles (LMs). LM behaves like a non-wetting solid which enables zero-loss transportation on solid surface and liquid pool. The challenge is controlling the liquid-releasing behavior, especially on the liquid pool. For example, releasing the inner liquid of LM at a specified time in adaptation to the liquid pool condition has not been achieved. In the past, different approaches were introduced to demonstrate instant release of inner liquid in presence of a specific stimulus—but the report on controlling the lifetime of floating LMs in presence of a stimulus is extremely rare in the literature. In this context, an inherently porous and crystalline nanomaterial, i.e., metal organic framework (MOF) is rationally transformed into a readily chemically reactive nanomaterial for associating both a) dual pH-responsive hydrophobicity and b) non-responsive superhydrophobicity through a 1,4-conjugate addition reaction. Further, the Kang-Jacobi wettability model was applied to examine the wettability transition of modified MOFs at various pH. The hydrophobic MOFs yielded LMs with the ability to automatically release inner liquid at a pre-defined time without requiring external intervention. Furthermore, the strategic association of protonizable amine, labile coordination bond and tailored hydrophobicity attributed to dual (acidic/alkaline) stimuli responsive adjustable life time of LMs on water pool. Such LMs were utilized for demonstrating 1) adjustable drug-release, 2) on-demand release of reactants to perform chemical reactions and 3) rapid optode detection of NO_2^-.

Introduction

Liquid marbles (LMs) are liquid droplets wrapped with micron/submicron-sized liquid repellent solid particles and aggregates.[1] The wrapping layer of mostly liquid repellent solid particles around the encapsulated liquid droplet provided an isolated and dry environment—and eventually protecting the LMs from contaminations.[1-3] The stability of such tiny and dry liquid droplets and their controlled bursting is essential for a wide range of practically relevant applications of LMs.[1-8] In the past, various particles with different shapes and sizes were explored to improve the stability of the LMs on both the solid/air and the liquid/air interfaces.[9-13] On the other side, in a seminal report, Fujii and coworkers introduced a stimuli-responsive LM through the strategic use of an alkaline steric stabilizer chain of a polymer latex particle.[4] The reported stimuli-responsive LM remained stable at the alkaline condition but readily collapsed on both the neutral and acidic water pool—due to the protonation induced switching of wettability of the polymeric latex particle. This work pioneered responsive LMs.[4,7] Inspired by this result, other stimuli-responsive LMs with the ability to immediately release the inner liquid at different monotonic stimuli—including alkaline condition, UV light, temperature, etc. are introduced thereafter.[4-5,7-8,14-15] In the recent past, LMs have been successfully applied in various relevant research topics—including miniaturized chemical reactions, loss-less transportation of liquid, tissue engineering, CO_2 capture, etc.[16-19] However, after significant progress on this research topic, the design of LMs with tuneable or even adaptive responsiveness, has not been achieved as reflected in Table 1. Various types of hydrophobic particles were introduced to demonstrate almost instant bursting of LMs in presence of specific stimuli—and such earlier reported approach remained inappropriate to adjust the lifetime of LMs in presence of respective stimuli as accounted in Table 1.[4,5,7,8,14,15,23,24,26,32-40] Thus, the report of mechanically robust LMs, having the ability

[a] *Bio-Inspired Polymeric Materials Lab, Department of Chemistry, Indian Institute of Technology-Guwahati, Kamrup, Assam 781039, India,*
E-mail: umanna@iitg.ac.in

[b] *Centre for Nanotechnology, Indian Institute of Technology-Guwahati, Kamrup, Assam 781039, India*

[c] *School of Healthcare Science & Technology, Indian Institute of Technology-Guwahati, Kamrup, Assam 781039, India*

[d] *International Center for Materials Nanoarchitectonics (MANA), National Institute for Materials Science (NIMS), Tsukuba, Ibaraki, Japan*
E-mail: TENJIMBAYASHI.Mizuki@nims.go.jp

Electronic Supplementary Information (ESI) available: [The attached supporting information accounting detailed experimental procedures and Figure S1 to Figure S20 accounting supplementary NMR spectra, measurements of wettability of chemically modified MOFs, transition of wettability on exposure to acidic and alkaline conditions, powder XRD and FESEM images of hydrophobic MOF after exposure to acidic and alkaline conditions, tolerance of liquid marbles under severe exposures, measurement of adsorption of chemically modified MOFs to aqueous phase at different pH]. See DOI: 10.1039/x0xx00000x

to a) automatically release the inner liquid at a precise and pre-defined time without having any external intervention and b) adjustable triggered bursting of the inner liquid on water pool in both acidic and alkaline conditions, is yet to be introduced in the literature. Such principally distinct design would likely to provide an elegant avenue for deriving functional soft materials for different fundamental and applied studies—including adjustable triggered drug release, on-demand chemical reaction and rapid chemical sensing etc.

In the past, the metal-organic framework (MOF) that was inherently associated with high crystallinity, porosity and surface area was strategically integrated with water-repellence property for improving structural stability and applied successfully in various potential applications related to energy, environment, catalysis, etc.[20-22] Recently, a few water-repellent MOFs were also explored to construct LMs[23-25]—but with no intention of designing programmable and triggered release of the inner liquid at the water pool. In the recent past, an amine-containing Zr based MOF, formally recognized as NH_2-UiO-66, was modified by strategically reacting the available amine and Zr-OH groups at harsh and complex chemical reaction conditions.[23,26-30]

In our current design, the strategic association of metal-organic framework and protonizable chemistry—in combination with tailored hydrophobicity is unprecedentedly introduced to design a LM with stimuli-responsive adjustable "lifetime till breakage" on a water pool. In this context, the prepared NH_2-UiO-66 was subjected to covalently react with trimethylolpropane triacrylate (3-Acl) to achieve readily chemically reactive MOF (CR-MOF, Scheme 1A-B). The residual

Table1. Comparing the stimuli-responsive bursting behaviour of current liquid marbles (LMs) with earlier reported LMs.

SN.	Materials	Modification	Selected stimuli for bursting of LMs	Adjustable bursting time under stimuli	Auto-bursting of LMs	Reference
1	Styrene beads	PDEA macromonomer	Acidic and neutral	No (Immediately)	No	4
2	Fe_3O_4 nanoparticle	Tetraethyl orthosilicate, (4-phenoxyphenyl)dip-henylsulfonium triflate, Poly(2-vinylpyridine-b-dimethylsiloxane) block copolymer	Acidic (<1.8) UV-light	No (Immediately)	No	5
3	Polypyrrole, carbon black	Octadecanoic acid	Near-infrared (NIR) light	No (< 20 Sec)	No	8
4	Silica nanoparticles	Methyl groups	------	------	------	14
5	TiO_2 particles, Fe_3O_4 particles	Triethoxy- [1H,1H,2H,2H-tridecafluoro-n-octyl]silane, Tetraethyl orthosilicate	UV-light	No (< 7 min)	No	15
6	Metal organic framework (NH_2-UiO-66)	Phenyl silane	------	------	------	23
7	Metal organic framework (UiO-66, UiO-67)	Perfuorooctanoic acid, Heptafuorobutyric acid	Water	No (Immediately)	No	24
8	Metal organic framework (ZIF-9-III ($[Co_4(bIm)_{16}]$)	……	------	------	------	26
9	Silica particle	poly(6-(acrylamido)hexanoic acid), 4-Cyanopenta- noic acid dithiobenzoate	Alkaline (> pH 9)	No (< 30 Sec)	No	32
10	Ferric chloride, polypyrrole	Heptadecafluorooctane sulfonic acid, Tridecafluorohexane-1-sulfonic acid potassium salt	Isopropanol vapour	No (Immediately)	No	33
11	Amino-carbon dots	Maleamic acid-isobutyl polyhedral oligomeric silsesquioxane (POSS)	------	------	------	34
12	Polymer particle	Heptadecafluorooctane sulfonic acid	IPA	No (Immediately)	No	35
13	Amino-carbon dots	Maleamic acid-isobutyl polyhedral oligomeric silsesquioxane (POSS)	------	------	-----	36
14	Stearic acid particle	Polypyrrole	IR Light and heating	No (< 30 s)	No	37
15	Chalcogenidometalate cluster	Alkyl groups	Volatile organic vapor	No (Few Seconds)	No	38
16	Graphene nanocolloid	……	-----	-----	------	39
17	Halloysite nanoclay	Octadecyl acrylate, Lauryl acrylate, Octyl acrylate, Hexyl acrylate	------	-----	Yes (~ 4 min to 60 min)	40
18	Amine-reactive metal organic framework	Decyl amine, Octyl amine, Hexyl amine, Pentyl amine	pH 1 to pH 12	Yes (0 min to 2.8 h)	Yes (1. 2 h to 2.8 h)	This work

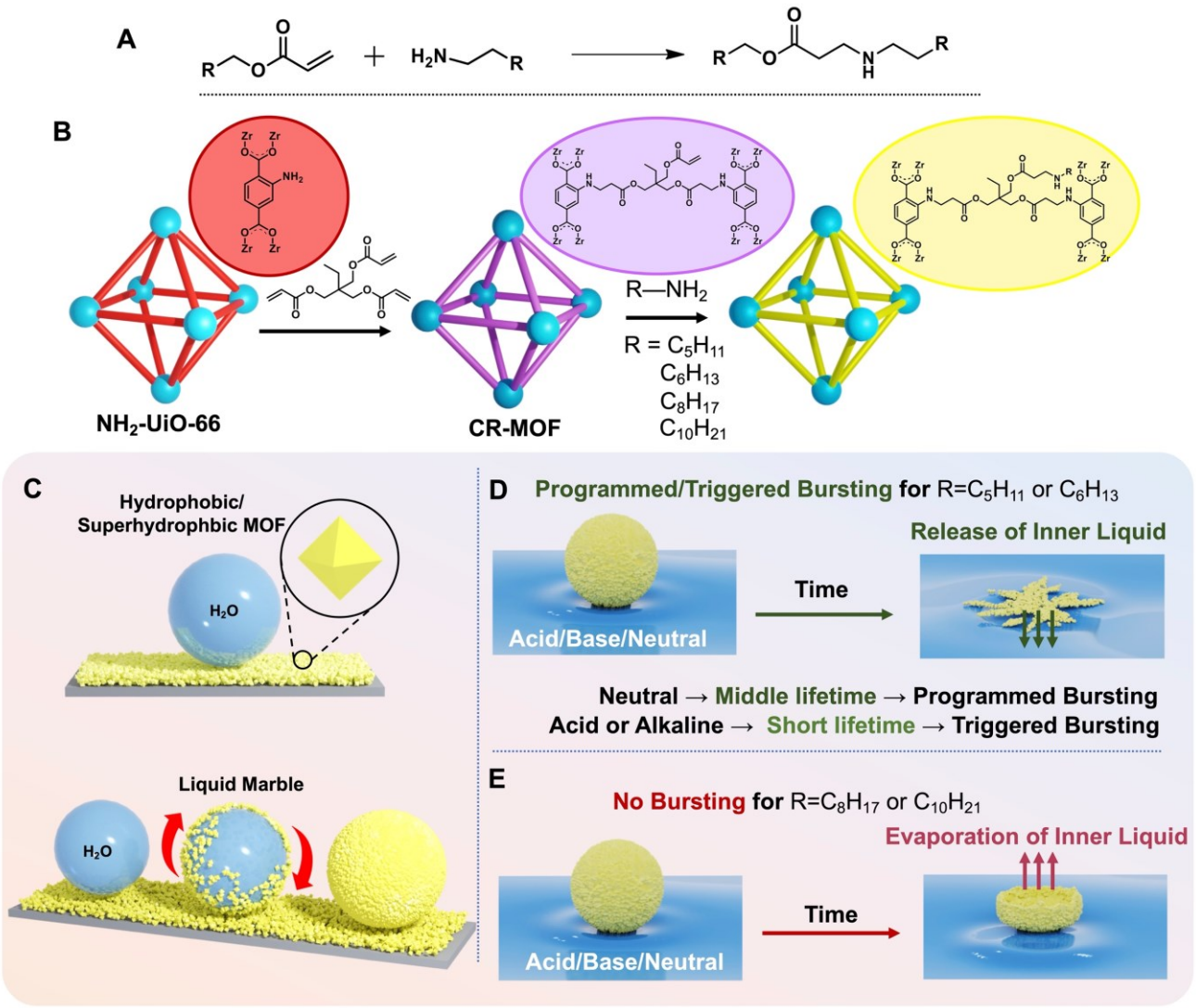

Scheme 1. A) Illustrating a catalyst-free 1,4-conjugate addition reaction between amine and acrylate. B) Accounting the conversion of prepared MOF (NH_2-UIO-66) into a chemically reactive MOF (CR-MOF) following the covalent modification with 3-Acl through 1,4-conjugate addition reaction. The residual acrylate group in CR-MOF provided a facile basis for post covalent modification with selected alkyl amines at ambient conditions to tailor water wettability (hydrophobicity and superhydrophobicity). C) Depicting the process of forming liquid marbles (LMs) by rolling the beaded water droplet on the pile of either hydrophobic or superhydrophobic MOFs. D) Schematic depicting the LMs prepared from hydrophobic MOFs displayed both programmed (moderate lifetime of liquid marble) and triggered release of inner liquid at water pool, without having any external intervention at neutral pH and in the presence of acidic/alkaline stimuli, respectively. E) Schematic depicting the LMs derived from superhydrophopbic MOFs failed to release inner liquid irrespective of the pH of the water pool, rather encapsulated water evaporated out from the LM.

acrylate reactivity of CR-MOF allowed to post-modify with selected alkyl amines following a common and facile 1,4-conjugate addition reaction at ambient conditions.[31] We hypothesized that the hydrocarbon tails of selected alkyl amine would modulate water repellence—and eventually control the exposure of available amines and labile coordination bond of the modified MOFs at the acidic and alkaline conditions, respectively. In fact, depending on the length of hydrocarbon tails in the selected alkyl (i.e., pentyl (-C_5H_{11}), hexyl (-C_6H_{13}), octyl (-C_8H_{17}) and decyl (-$C_{10}H_{21}$)) amine, the modified MOFs provided either dual (acid/alkaline)-responsive (pentyl, hexyl) or non-responsive (octyl, decyl) water repellence (hydrophobicity/superhydrophobicity). Covering the water droplet with such chemically modulated MOF (Scheme 1C), we aimed to introduce a new class of responsive LMs that provides an automated (at neutral condition) and adjustable (depending on pH) triggered release of inner liquid at the water pool, as shown in Scheme 1D. The choice of chemical modulation decides the floating time of the same LM at acidic and alkaline conditions (Scheme 1D-E).

Results and Discussion

Developing Chemically Reactive Metal Organic Framework

In the recent past, automated bursting of LMs—without demanding any external intervention was introduced by strategically modifying the halloysite nanoclay with different alkyl acrylate, where embedded hydrophobicity of modified

nanoclay controls the diffusion length of water vapour across the LM's shell to control the lifetime of floating LMs.[40] Here, a completely distinct approach is adopted to design of chemically reactive MOF for precisely control the wettability transition from hydrophobicity to hydrophilicity through i) triggering the structural instability of MOF in alkaline condition and ii) protonating the available amine moiety in the modified MOF at acidic condition. This simple principle is extended to achieve both automated (at neutral condition) and adjustable (depending on pH) triggered release of inner liquid from LMs at water pools. In this relevance, the NH_2-UiO-66 was prepared and characterized with ^{1}H NMR, powder XRD and FESEM studies (Figures S1, and 1) prior to covalently reacting with trimethylolpropane triacrylate (3-Acl) through the 1,4-conjugate addition reaction. The resultant MOF is loaded with residual acrylate groups which makes it chemically reactive—and such MOF is denoted as CR-MOF. The covalent modification of NH_2-UiO-66 with 3-Acl and the existence of residual acrylate groups were characterized with ^{1}H NMR study. After the mutual reaction between prepared NH_2-UiO-66 and 3-Acl, the ^{1}H NMR spectrum of the HF/DMSO-d_6-digested product (CR-MOF; Fig. S2) displayed peaks at δ= 7.10 (d), 7.27 (s) and 7.87 (d) ppm, corresponding to the aromatic protons of the MOF. Furthermore, four sets of triplets at δ= 2.57, 2.63 ppm and δ= 3.45, 3.49 ppm appeared in the aliphatic region, which correspond to the β- and α-protons to the two chemically different secondary amine, respectively. Additionally, the three sets of doublet of doublet at 5.87 (dd, *J* = 10.3, 1.6 Hz, for cis & germinal coupling), 6.25 (dd, *J* = 17.2, 1.6 Hz, for trans & germinal coupling) and 6.07 (dd, *J* = 17.2, 10.3 Hz, for trans & cis coupling) ppm can be found which correspond to the remaining vinylic protons of the 3-Acl. The peaks at 1.17 (t, 3H) and 2.73-2.70 (m, 2H) correspond to the aliphatic ethyl group. However, the peaks for three aliphatic -CH_2 groups (assigned by 6 & 7 in the NMR spectrum) at the region 4.0-4.5 ppm are merged with the broad peak arising due to HF used. The integral intensity ratio of aromatic proton to vinyl proton is found to be 2/1 as two thirds of acrylate groups of one 3-Acl are mutually reacted with amines of two ligands, i.e. H_2ATA. The third acrylate group of 3Acl remained unreacted to NH_2-UiO-66—likely due to the existence of steric hindrance imposed by reacted MOF around the 3Acl molecule. Thus, the unreacted acrylate moiety makes

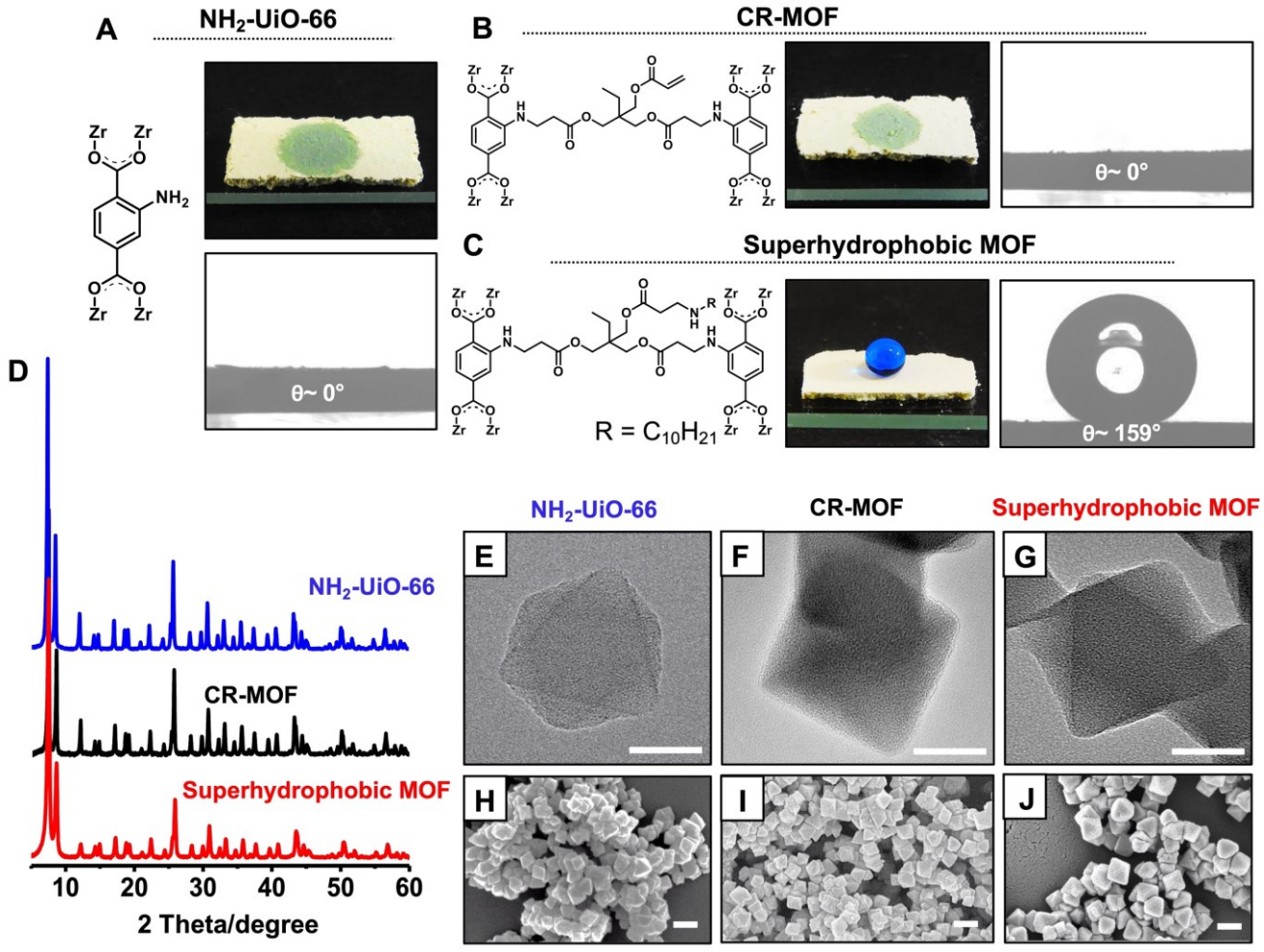

Figure 1. A-C) The digital images and contact angle images accounting for water wettability of NH_2-UiO-66 (A), CR-MOF (B) and superhydrophobic MOF (C). D) Powder XRD pattern of NH_2-UiO-66 (red), CR-MOF (black) and superhydrophobic MOF (blue). E-J) Field emission transmission electron microscope (FETEM; E-G, scale bar, 50 nm) and field emission scanning electron microscope (FESEM; H-J, scale bar, 100 nm) of NH_2-UIO-66 (E,H), CR-MOF (F,I) and superhydrophobic MOF (G,J).

the prepared MOF readily chemically reactive at ambient conditions. The reaction duration provides a facile basis to control the content of residual acrylate groups in CR-MOF (Fig. S3). Further, the residual acrylate group present in CR-MOF was exploited to post-modify with desired amine-containing alkyl chain. In this context, the post-covalent modification of CR-MOF with pentyl amine was successfully characterized with ^{1}H NMR spectral analysis. After the reaction with pentyl amine, the ^{1}H NMR spectrum of the HF/DMSO-d_6-digested product (Fig. S4) showed the appearance of new peaks at δ= 0.87 (t, 3H), 1.32-1.25 (m, 4H), 1.57-1.50 (m, 2H) and 2.91- 2.88 (m, 2H) for the aliphatic protons of pentyl group and two new methylene protons (10 & 11 in the NMR spectrum). During this mutual chemical reaction between amine and acrylate, the vinyl moiety converted into methylene moiety. Out of these two methylene protons, one is raised separately at 3.10 ppm (t, 2H) and the other is merged with one of the β protons of secondary amine at 2.63 ppm (t, 4H) due to the nearly similar chemical environment of the protons. This is supported by the integral intensity of the peaks at that particular region. In addition, a significant depletion of the ^{1}H-NMR signal for the residual acrylate group in the range from 6.25 ppm to 5.87 ppm was noted with respect to the aromatic protons (δ= 7.10 (d, 2H), 7.27 (s, 2H) and 7.87 (d, 2H) ppm) as shown in Figure S3. This data unambiguously indicated the post-covalent modification of CR-MOF with selected pentylamine. Furthermore, FTIR spectral analysis supported that the mutual reaction between 3-Acl and NH_2-UiO-66 yielded CR-MOF, where IR signatures for carbonyl stretching and C-H deformation of vinyl group appeared at 1722 cm^{-1} and 1411 cm^{-1}, respectively. On treating the CR-MOF with pentylamine, the characteristic IR peak for aliphatic C-H stretching of pentyl moiety was noticed as shown in Figure S5.

Eventually, such a facile chemical modulation strategy allowed to tailor a range of desired water wettability of the prepared MOF (Figure 1A-C). For example, the post-covalent modification of the CR-MOF with decyl amine (DA) yielded a superhydrophobic MOF with a water contact angle (WCA) of ~159°, as shown in Figure 1C. The impact of other modifications on the water wettability to achieve degrees of hydrophobicity is discussed later. Importantly, the integration of the residual acrylate group in the NH_2-UiO-66 and the subsequent post-covalent modification of CR-MOF have minimal impact on the structural integrity of the native MOF, as evident from the similarity in the powder XRD pattern of native MOF, CR-MOF and superhydrophobic MOF, as shown in Figure 1D. Similarly, the morphology of the native MOF remained unaffected after the association of residual acrylate groups and its post-covalent modification with DA through the 1,4-conjugate addition reaction, as confirmed from both FETEM and FESEM images in Figure 1E-J. The octahedral shape was preserved in the highly

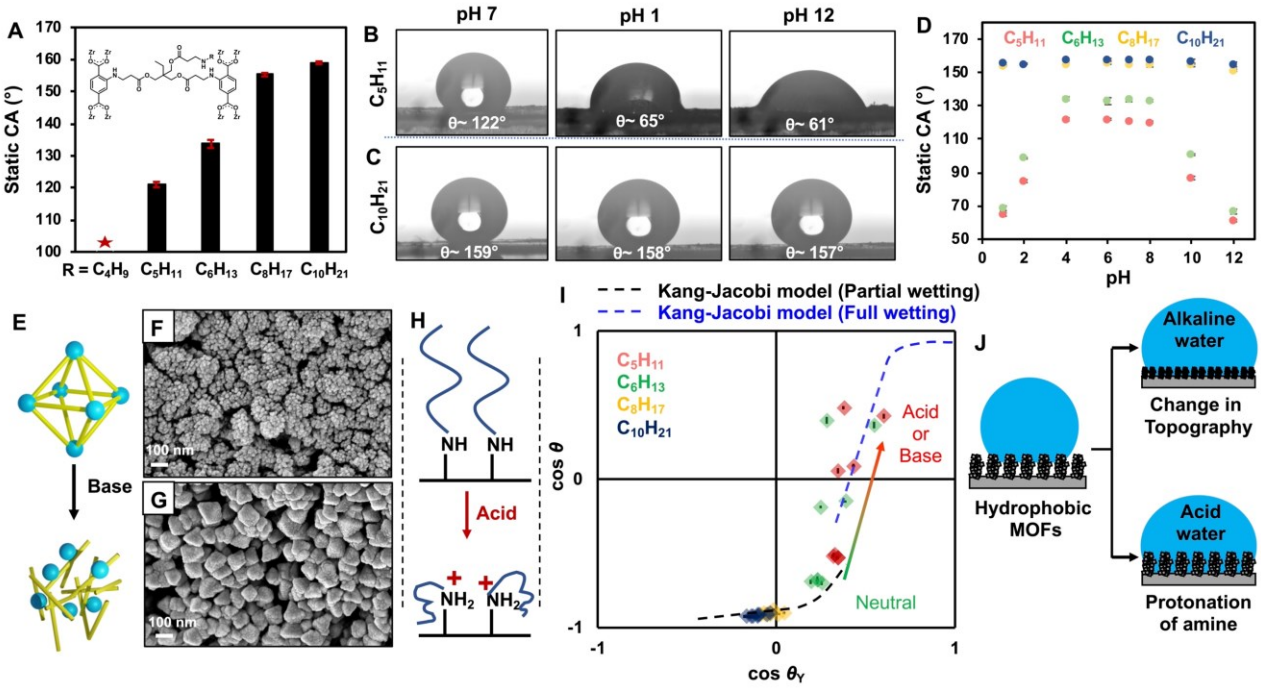

Figure 2. A) The plot accounting for the change in water wettability of the modified MOFs depending on the hydrocarbon tail length of selected modifiers, i.e., alkyl amines. B) Contact angle images illustrating the water wettability of hydrophobic (modified with pentyl amine: –C_5H_{11}) and superhydrophobic (modified with decyl amine: –$C_{10}H_{21}$) MOFs at neutral (pH 7), acidic (pH 1) and alkaline (pH 12) conditions. D) Plot depicting the changes in water wettability of differently modified hydrophobic and superhydrophobic MOFs having distinct hydrocarbon tails (C_5H_{11}, C_6H_{13}, C_8H_{17} and $C_{10}H_{21}$) at various pH (from 1 to 12). E) Schematic depicting the collapse of the structural integrity of hydrophobic MOFs at alkaline condition. F-G) FESEM images of PA-modified hydrophobic MOF after the alkaline (pH 12, F) and acidic (pH 1, G) pH exposures. I) Kang-Jacobi wettability model illustrating the wettability transition of both hydrophobic and superhydrophobic MOFs at various pH. J) The schematic depicting the alteration of wettability of hydrophobic MOFs at alkaline and acidic condition through the change in topography and protonation of amine.

crystalline MOF, irrespective of associating these distinct chemical modulations.

MOF with Chemically Tailored Water Wettability

For the controlled tailoring of water wettability, the chemically reactive MOF was post-modified with various alkyl amines, i.e., lower analogues of DA—and the hydrophobicity of the MOF was gradually depleted with reducing the length of the hydrocarbon tail of the selected alkyl amine from —$C_{10}H_{21}$ (DA) to —C_5H_{11} (pentyl amine, PA) as shown in Figure 2A. While individual modifications of CR-MOF with octyl amine (OA) and DA provided superhydrophobicity with a WCA > 150°, the modification of the same MOF with hexyl amine (HA) and PA provided only hydrophobicity with WCA of ~133° and ~121° respectively. However, the post-covalent modification with butylamine (BA) failed to alter the water wettability—and it remained highly hydrophilic, as shown in Figure S6. Thus, the water wettability of the octahedral shaped MOF was tailored through the facile and catalyst-free 1,4-conjugate addition reactions with appropriate alkyl amine at ambient conditions. Thereafter, the impact of pH on the chemically modified MOF was examined. Interestingly, the PA (—C_5H_{11}) modified hydrophobic MOF displayed a drastic and instant transition in water wettability from hydrophobicity (WCA of 122°) to hydrophilicity (<70°) in both highly acidic (pH 1) and alkaline (pH 12) conditions, however superhydrophobic MOF (DA-treated) remained non-responsive to the extremes of pH, instead it continued to exhibit unperturbed superhydrophobicity with WCA > 155°, as shown in Figure 2B and Figure S7. Thereafter, the water wettability of differently chemically-modulated (PA, HA, OA) hydrophobic and superhydrophobic MOFs were examined in various pH over a range from pH 1 to pH 12, as shown in Figure 2D. We observed no instant change in water wettability for the hydrophobic MOFs at the pH range of 4 to 8—however, a significant depletion of the WCA was noted at highly acidic (pH 1 & 2) and alkaline (pH 10 & 12) conditions, as shown in Figure 2D. Whereas the superhydrophobic MOFs displayed uninterrupted water repellence with WCA of > 150°

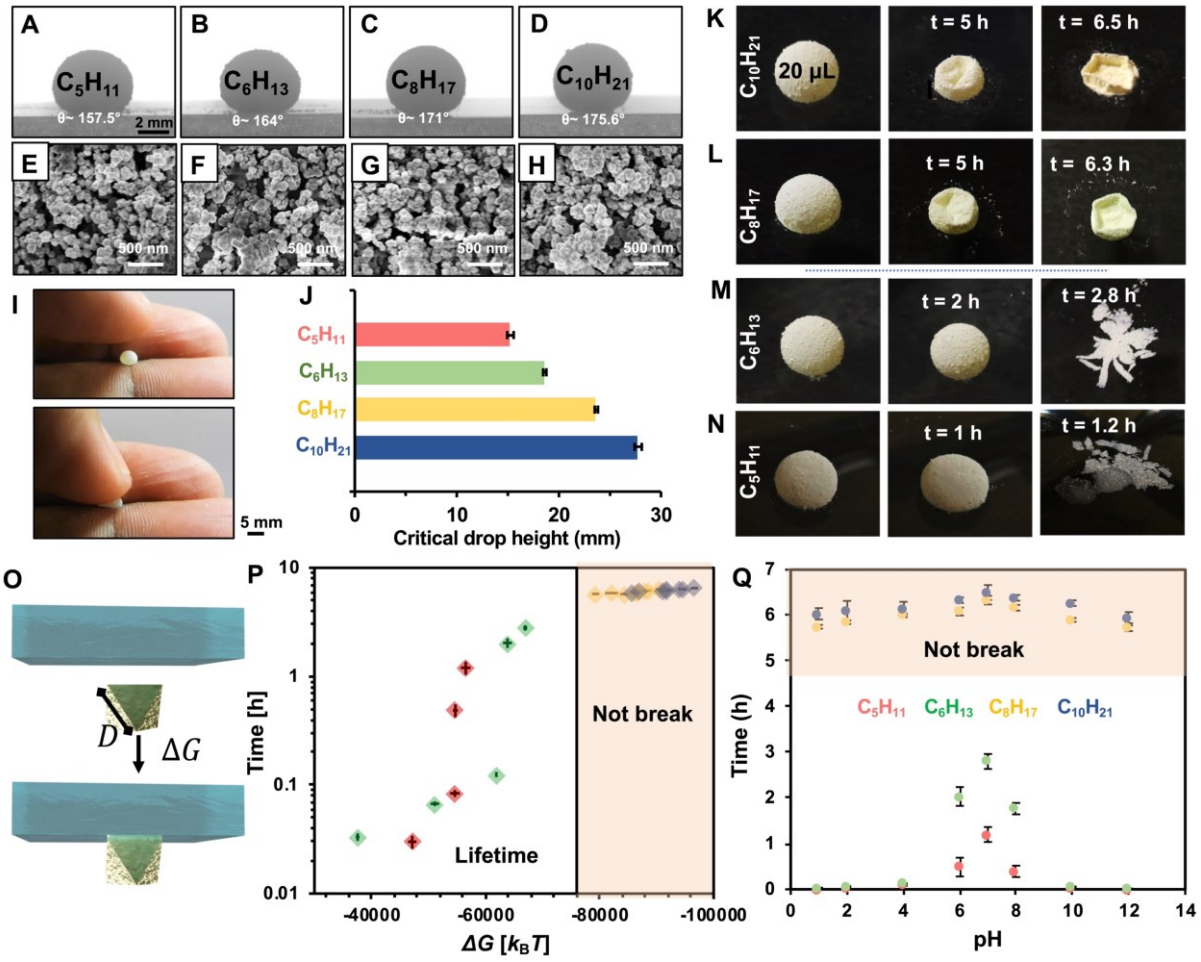

Figure 3. A-D) Contact angle images of LMs that were prepared with different alkyl amine modified MOFs, the contact angle improves with increasing the hydrocarbon tails (C_5H_{11}, C_6H_{13}, C_8H_{17} and $C_{10}H_{21}$) of modified MOFs. E-H) FESEM images illustrating the arrangement of MOFs (that were decorated with various alkyl amines (E: PA, F: HA, G: OA and H: DA)) at air/water interface, where the superglue (cyanoacrylate) is used to preserve the arrangement of respective MOFs at air/water interface. I) Digital images illustrating the compressive deformation of the prepared LM with bare fingers. J) Plot to account for the impact durability of prepared LMs, where LMs were dropped from a certain height that they can survive. K-N) Digital images illustrating the buckling and bursting of LMs that were prepared from differently modified superhydrophobic (K-L) and hydrophobic (M-N) MOFs. O) Illustrating the energy of adhesion of MOF. P) Accounting the dependence of the lifetime of LMs on the energy of adhesion of chemically modified MOF. Q) Accounting the stability of LMs at various pH of the water pool.

over a pH range from 1 to 12. Thus, the same CR-MOF individually post-modified with selected alkyl amine resulted in dual (acidic/alkaline) pH-sensitive hydrophobicity and uninterrupted superhydrophobicity.

To understand such distinct wettability transitions for hydrophobic and superhydrophobic MOFs in various pH, further experiments were designed. In the past, the structural instability of NH_2-UiO-66 at alkaline condition was addressed through the association of superhydrophobicity. Similar to the previous report, the currently synthesized superhydrophobic MOF continued to display unperturbed extreme water repellence at extremes of pH—with no change in structural integrity even after exposure to extremes of pH for 6 h as evident from the powder XRD pattern in Figure S8. However, the PA-modified hydrophobic MOF failed to protect the structural integrity of the MOF (Figure 2E) at the alkaline condition, as evident from the powder XRD pattern (Fig. S8). The octahedral shape of the MOF was distorted entirely—and the appearance of random granular domains after the alkaline treatment indicated the damage of the structural integration of hydrophobic MOF as shown in Figures 2F and S10. Thus, the structural instability contributed to the transition of water wettability of the PA treated MOF from hydrophobicity to hydrophilicity at alkaline conditions. However, the same hydrophobic MOF that was treated at highly acidic (pH 1) condition, continued to display the octahedral morphology (Figure 2G)—with unaffected crystallinity, as evident from the existence of indistinguishable powder XRD pattern to that of native MOF in Figure S8. On exposure of modified MOF to alkaline condition, the characteristic IR signatures—including $v_{asym}[COO^-]$ (1569 cm^{-1}), $v_{sym}[COO^-]$ (1382 and 1436 cm^{-1}) were disappeared, whereas these peaks remained intact even after exposure to neutral and acidic condition (Figure S9). This study revalidated the disintegration of modified MOF selectively at alkaline condition. In acidic exposure, the available amine group in the hydrophobic MOF is likely to be protonated—and resulted in the change in wettability from hydrophobic to hydrophilic as shown in Figure S3. Thereafter, the water wettability of both hydrophobic and superhydrophobic MOFs was investigated at various pH and the obtained data were fitted with the Kang-Jacobi model of wettability, as shown in Figure 2I. As expected, the superhydrophobic MOFs followed the partial wetting (i.e., the air layer is entrapped beneath the droplet) of the Kang-Jacobi model—whereas the hydrophobic MOFs displayed a transition from partial wetting to full wetting (i.e., the entrapped air layer diminished) depending on changing the environment from neutral to acidic or alkaline as depicted in Figure 2J. Thus, the chemically modulated hydrophobic MOF displayed from both a) the structural instability in alkaline condition and b) the protonation of available amine in acidic condition,—which eventually provided a facile basis to derive an adaptive LMs with the ability of both automated and adjustable triggered release of inner liquid. However, the superhydrophobic MOFs absolutely failed to display such characteristics as the available amine and labile coordination bonds are likely to be buried by the long hydrocarbon tails of the superhydrophobic MOFs.

Deriving Adaptive Liquid Marble

Both the dual (acidic/alkaline) pH-responsive hydrophobic and non-sensitive superhydrophobic MOFs were explored in preparing LMs by wrapping the water droplet with the respective hydrophobic and superhydrophobic MOFs. In Figure 3A-D, the MOF LMs sit on the hydrophilic glass substrate with an apparent contact angle of >150°, like a superhydrophobic state (Fig. S11). The contact angle is gradually increased with the increase in the chemically modulated hydrophobicity of the modified MOF. The higher contact angle is attributed to the shell tension of the LMs, which resist the deformation caused by the LMs' weight. After that, the surface structures of LMs are obtained by polymerizing their air–water interface[41] and then observed by FESEM (Figure 3E-3H), where no apparent change in the structure of LMs surface is observed. We hypothesize that the molecular interaction between MOFs contributes to the change in the LMs tension. In that, the interaction among modified MOFs improved with increasing the length of the hydrocarbon tail. The MOF derived LMs exhibit tolerance against mechanical compression (Figure 3I, Figure S12, Movie 1) manipulations with bare hands (Figure S13, Movie 2) and impact on the solid surface (Figure 3J, Figure S14, Movie 3). The mechanical strength and survival under compressive strain improved with the embedded hydrophobicity (Figure 3J and Figure S10M) of modified MOF. Eventually, the improved hydrophobicity of MOF contributed to resisting inner liquid spill from the prepared LMs.

Then, these LMs were placed onto the water pool to examine their lifetime (Figure 3K-3N). We find that the lifetime of the LMs drastically changed with the variation in the embedded hydrophobicity. In that, LMs derived from OA ($–C_8H_{17}$) or DA ($–C_{10}H_{21}$) modified MOF did not collapse until the inner liquid evaporated completely (Figure 3K, 3L), whereas LMs prepared out of HA ($–C_6H_{13}$) or PA ($–C_5H_{11}$) modified MOF collapsed down with a lifetime of 1.2 or 2.4 hours, respectively (Figure 3M and 3N). To understand the stability of LMs that are derived from chemically modulated MOFs, we considered the free energy ΔG required to adsorb a single MOF to the water surface (Figure 3O), which yields:

$$\Delta G = -\sqrt{3}/4D^2[1 + \cos\theta_Y]$$

where D is the one side length of the MOF, γ_L is the inner liquid surface tension, and ϑ_Y is the Young contact angle of the inner liquid droplet on the MOF surface (see details for supporting information). Here, ϑ_Y on the MOF is substituted by the static contact angle on the flat glass substrate coated with the same chemicals used for MOFs' modification (Figure S15). We assume that the one face of the MOF with the surface area of $\sqrt{3}/4D^2$ attach to the water surface, which results in the formation of the MOF–water interface while decreasing the MOF–air and water–air interfaces. Thus, we obtain

$$\Delta G = -\sqrt{3}/4D^2[\gamma_S + \gamma_L - \gamma_{SL}]$$

where γ_S and γ_{SL} are MOF–air and MOF–water interfacial energy. According to Young equation, $\gamma_S = \gamma_L \cos\theta_Y + \gamma_{SL}$. By combining these equations, we obtain

$$\Delta G = -\sqrt{3}/4D^2[1 + \cos\theta_Y]$$

We observed that the LMs' lifetime was increased with the decrease of the adsorption energy, and the LM with the *ΔG* smaller than the threshold value was not broken down in this experiment (Figure 3P).

We noticed that the MOFs' pH responsivity modulates their wettability (Figure 2D) and/or size (Figure 2F, 2G) as well as their *ΔG* (Figure S16). Thus, the lifetime of the same MOF based LM is also varied in response to the water pool's pH (Figure 3Q). However, the lifetime of the LM on water pools mostly depends on the chemical modification of the prepared CR-MOF with

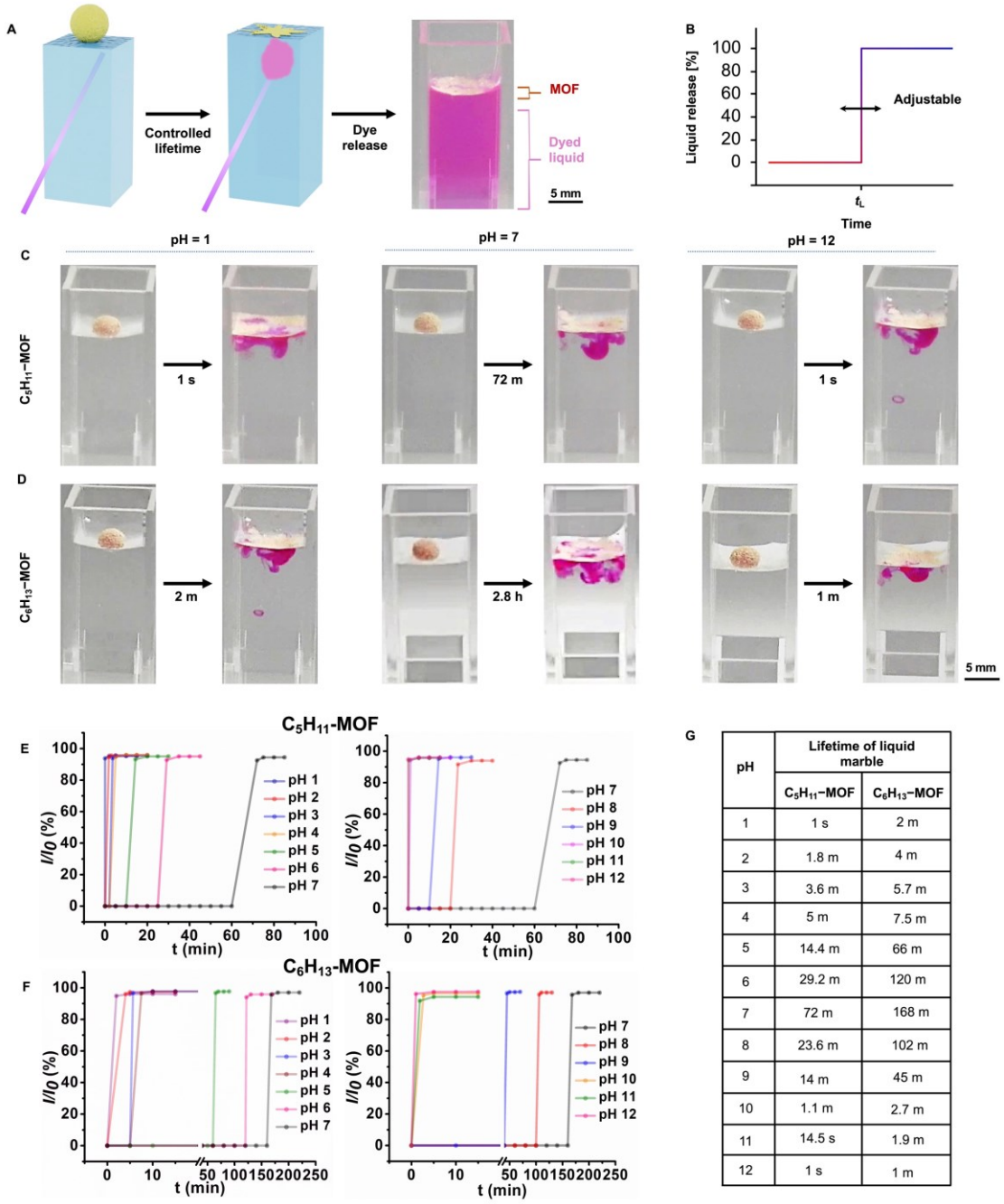

pH	Lifetime of liquid marble	
	C_5H_{11}–MOF	C_6H_{13}–MOF
1	1 s	2 m
2	1.8 m	4 m
3	3.6 m	5.7 m
4	5 m	7.5 m
5	14.4 m	66 m
6	29.2 m	120 m
7	72 m	168 m
8	23.6 m	102 m
9	14 m	45 m
10	1.1 m	2.7 m
11	14.5 s	1.9 m
12	1 s	1 m

Figure 4. A) Illustrating the release of loaded solution of dye through controlled bursting of LMs. B) Depicting the adjustable release of loaded liquid by modulating the life time of the prepared LMs. C-D) Digital images demonstrating the release of loaded rhodamine B from LMs that were prepared using pentyl (C) and hexyl (D) modified MOF at hour, minutes and second scales depending on the pH (1, 7 and 12) of the aqueous media. E-F) The plots accounting the percentage of change in absorption intensity due to release of dye from respective LMs (pentyl and hexyl modified MOF based) in aqueous phase at different acidic (pH =1, 2, 3, 4, 5 and 6) and alkaline (pH =8, 9, 10, 11 and 12) conditions and the adjustment of release of dye from same LMs (either pentyl-modified MOF: E or hexyl modified MOF: F) are compared with respect to neutral pH condition. G) Accounting the life time of different LMs at various pH of the water pool.

selected alkyl amines. On the other side, the LMs prepared from differently modified MOFs did not collapse to release inner liquid on solid surface rather the encapsulated water evaporated over the time—which resulted in the buckling of the prepared LMs (Figure S17).

Carrier for Adjustable Drug-Release

Taking advantage of the pH-dependent lifetime of the PA and HA-modified MOFs at both acidic and alkaline conditions, we demonstrated the adjustable drug release, where rhodamine B (2 mM) is selected as a model drug molecule (Figure 4A-B) for visualizing the inner liquid release, and the concept can be applied to the drug release application. The dissolved model drug molecule is encapsulated in the LMs—and controlled bursting of LMs allows the release of loaded rhodamine B at a specified time as depicted in Figure 4A. At neutral pH (7), the release of the loaded solution of rhodamine B from LMs that were separately prepared using PA and HA-modified MOFs was noticed after 72 min and 2.4 h, respectively, as shown in Figure 4C-D. However, the same LMs rapidly released the loaded solution of dye at both pH 1 and pH 12—and the time scale for releasing the loaded solution of dye was reduced from 72 minutes to 1 second and 2.8 h to 1 or 2 minutes for PA and HA modified MOF based LMs, respectively, as shown in Figure 4C-D. Thereafter, the release of loaded dye molecules from the same LMs at various other pH was monitored by measuring the change in the percentage of absorption intensity over time. Depending on the pH of the water pool and chemical modification of the MOFs that were used to prepare the respective LMs provided an adjustable release of loaded drug molecules from LMs as shown in Figure 4E-F. The LMs remained efficient to adjust the triggered release time—depending on the selection of either acidic or alkaline pH of the media. It is because of the alteration of lifetime of different LMs at various pH of the aqueous pool (Fig. 4G). Eventually, such chemically modulated MOF-based LMs can act as a carrier for the time-programmed release of the loaded molecules at different pHs. It is worth mentioning that the lifetime of these LMs slightly improved on increasing the ionic strength of the water pool by adding salt (NaCl, Figure S18), where the depleted vapour pressure is expected to improve the stability of LMs.

Triggered Chemical Reaction at Water Pool

This section summarizes the behaviour of the MOF-based LMs placed on a water pool as shown in Figure 5A-4D. The HA ($–C_6H_{13}$) or PA ($–C_5H_{11}$) modified MOF-based LMs broke down on the water pool after a few hours in the neutral condition, and the lifetime could be shortened by the variation in the pH of the water pool (Figure 5A and 5C). Whereas LMs prepared from OA ($–C_8H_{17}$) or DA ($–C_{10}H_{21}$) modified MOF were not collapsed at any of these pHs (Figure 5B, 5D). Such multi-responsivity in LMs on water pools has not yet appeared in the literature. Using the feature of the MOF-based LMs, time-programmed inner liquid release on the water pool was possible under acidic (Figure 5E, Movie 4) or alkaline conditions (Figure 5F, Movie 5). In the setup, LMs prepared by different hydrophobic MOFs were placed on the water pool, and the concentrated aqueous solution of acid or base was added into the water pool. In both cases, LM

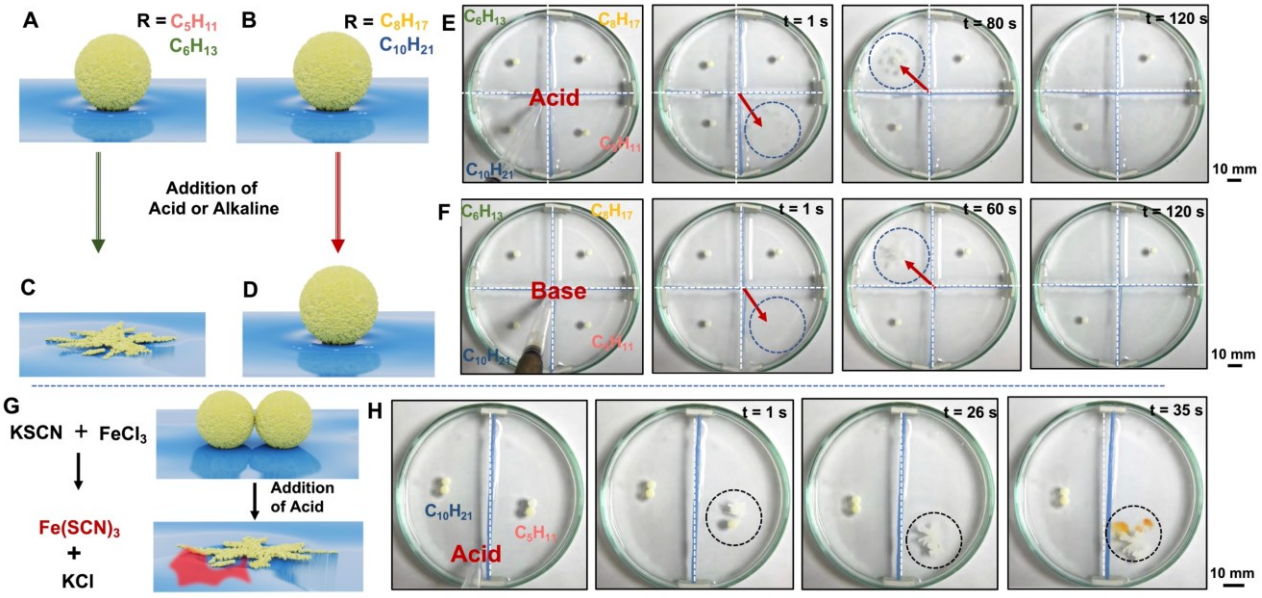

Figure 5. A-D) Schematic illustrating the acid/alkaline-responsive (A,C) and non-responsive (B,D) behaviour of LMs at water pool. The LMs were prepared from hydrophobic (decorated with C_5H_{11} and C_6H_{13}; A) and superhydrophobic (modified with C_8H_{17} and $C_{10}H_{21}$; B) MOFs. C) Hydrophobic MOFs based LMs displayed bursting at the water pool at both acidic and alkaline exposures, whereas LMs derived from superhydrophobic MOFs remained unperturbed at both acidic and alkaline water pool (D). E-F) Digital images demonstrating the spatially selective triggered release of inner liquid from LMs that were prepared from hydrophobic MOFs in the presence of both acidic (E) and alkaline (F) conditions, the LMs that were derived from superhydrophobic MOF failed to burst at identical setups. G-H) Demonstrating the triggered chemical reaction on the water pool in the presence of acidic stimuli by individual and triggered release of mutually reactive reactants (ferric chloride and potassium thiocyanate) from two LM prepared from hydrophobic MOF. The formation of ferric thiocyanate complex resulted in the appearance of red colour in the water pool. However, LMs that were prepared from superhydrophobic MOF failed to release the encapsulated reactants at the identical setup.

derived from hydrophobic MOFs readily broke down to release the inner liquid into the water pool. As expected, the LM derived from PA ($–C_5H_{11}$) modified MOF was broken faster (~ 1 minute) than the LM prepared from HA ($–C_6H_{13}$) modified MOF. These phenomena could be used for demonstrating on-demand chemical reactions at the water pool (Figure 5G). For this purpose, the PA ($–C_5H_{11}$) modified LMs were formed by KSCN (aq.) or $FeCl_3$ (aq.) solutions. In response to the acid added to the water pool, they collapsed to release solutions of mutually reactive reactants. The water gets red colored due to the formation of metal complexes through the mutual reaction between selected metal ions and ligands (Figure 5H, Movie 6). During this reaction, the DA($–C_{10}H_{21}$) modified LMs were not broken down and instead kept floating in the water. The formation of a metal ion complex is characterized by UV-Vis spectral characterization (Figure S19). Moreover, such demonstration of chemical reaction may be extended to other solvent systems and reactants as the modified MOFs allowed to prepare LMs using liquids with different surface tension as shown in Figure S20.

Optode Detection of Nitrite Ion (NO_2^-) in Water

In this section, the acid-triggered bursting behaviour of prepared LM is successfully applied to sense an important and relevant toxic chemical—i.e., nitrite ions (NO_2^-). Consumption of NO_2^- contaminated water beyond a certain concentration (65 μM recommended by the World Health Organization (WHO)) is known to have a severe impact on our health.[42-43] Here, the stimuli-responsive LM was utilized to demonstrate optode detection of NO_2^- below its recommended concentration. In this context, reagents for modified Griess reactions,[44] i.e., sulfanilamide and aniline, were loaded in the prepared LM prior to placing it in a water pool contaminated with NO_2^- (40 μM). Upon addition of HCl, the water pool became acidic and the LM collapsed to release the loaded reagents to undergo Griess reaction in the presence of NO_2^-. Immediately, the color of the water poll turned yellow as shown in Fig. 6A and Movie 7. However, we have not noticed such changes in coloration in the water pool—in the absence of nitrite ions as shown in Fig. 6B and Movie 8. The modified Griess reaction between released reagents (sulfanilamide and aniline) from LM and nitrite ions present in the water pool at acidic condition yielded the yellow colored diazo dye as shown in Figure 6C. The appearance of IR peak for N=N stretching at 1552 cm^{-1} revealed the formation diazo compound as shown in Figure 6D.[45] Thus, the current strategy is successfully implemented for proof of concept demonstration of the naked eye, fast and facile detection of nitrite ions well below its recommended concentration.

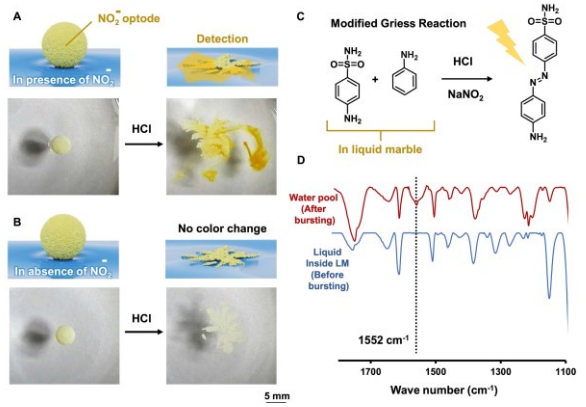

Figure 6. A) Depicting the optode sensing of nitrite ions on acid-triggered bursting of the prepared LM (loaded with sulfanilamide and aniline) in water pool contaminated with nitrite ions, where water pool became yellow in color. B) No such color change is noted in absence of nitrite ion in the water pool. C) Represents the reaction scheme for modified Griess reaction. D) FTIR spectra of loaded aqueous phase in LM (before bursting) and the coloured water pool after bursting of LM.

Conclusions

In conclusion, here, we have introduced a chemically reactive and porous nanomaterial for controlled and precise chemical modulation through a 1,4-conjugate addition reaction at ambient conditions to derive mechanically robust LMs with tuneable and adaptive pH sensitivity. While chemically modulated and inherently porous MOFs decorated with longer hydrocarbon tails provided physically and chemically tolerant LMs, the association of shorter hydrocarbon tails yielded LMs for the automated releasing of inner liquid at the water pool at a predefined time (order of hours)—without external intervention. In fact, the selected chemical modulation of MOF controls the lifetime (from seconds to hours) of LMs at both acidic and alkaline conditions. Such principle was successfully exploited to demonstrate 1) predetermined automated bursting of inner liquid on a water pool and triggered release of mutually reactive chemicals to perform chemical reaction on demand, 2) adjustable small molecule release and 3) facile and fast chemical sensing.

Acknowledgements

We thank Science and Engineering Research Board (CRG/2022/000710) and Ministry of Electronics and Information Technology (no. 5(1)/2022-NANO) and DBT (BT/PR45283/NER/95/1919/2022) for financial support. We also acknowledge the support from DST (DST-FIST programme; Sanction No. SR/FST/CS-II/2017/23C). We thank CIF, CFN, SHST and Department of Chemistry, Indian Institute of Technology-Guwahati, for their generous assistances in executing various experiments and for the infrastructures. SK and NB thank the institute and MoE for her PhD fellowship. AB acknowledges CSIR for the doctoral fellowship. We acknowledge the kind help of Mr. Avijit Mondal and Prof. Dipankar Srimani on NMR spectral analysis.

References

1 P. Aussillous and D. Quere, *Nature*, 2001, **411**, 924-927.
2 Y. Xue, H. Wang, Y. Zhao, L. Dai, L. Feng, X. Wang and T. Lin, *Adv. Mater.*, 2010, **22**, 4814–4818.

3 C. H. Ooi, R. Vadivelu, J. Jin, K. R. Sreejith, P. Singha, N.-K. Nguyen and Nam-Trung Nguyen, Lab Chip, 2021, **21**, 1199.
4 D. Dupin, S. P. Armes and S. Fujii, *J. Am. Chem. Soc.*, 2009, **131**, 5386–5387.
5 L. Zhang, D. Cha and P. Wang, *Adv. Mater.*, 2012, **24**, 4756–4760.
6 D. Wang, L. Zhu, J.-F. Chen, and L. Dai, *Angew. Chem. Int. Ed*., 2016, **55**, 10795-10799.
7 S. Fujii, S.-I. Yusa and Y. Nakamura, *Adv. Funct. Mater.*, 2016, **26**, 7206–7223.
8 M. Paven, H. Mayama, T. Sekido, H.-J. Butt, Y. Nakamura and S. Fujii, *Adv. Funct. Mater.*, 2016, **26**, 3199.
9 P. S. Bhosale, M.V. Panchagnula and H. A. Stretz, *Appl. Phys. Lett.*, 2008, **93**, 034109.
10 F. Geyer, Y. Asaumi, D. Vollmer, H.-J. Butt, Y. Nakamura and S. Fujii, *Adv. Funct. Mater.*, 2019, **29**, 1808826.
11 Z. Liu, Y. Zhang, C. Chen, T. Yang, J. Wang, L. Guo, P. Liu and T. Kong, *Small*, 2019, **15**, 1804549.
12 Y. Asaumi, M. Rey, K. Oyama, N. Vogel, T. Hirai, Y. Nakamura and S. Fujii, *Langmuir*, 2020, **36**, 13274-13284.
13 M. Tenjimbayashi and S. Fujii, *Small*, 2021, **17**, 2102438.
14 M. Anyfantakis, V. S. R. Jampani, R. Kizhakidathazhath, B. P. Binks and J. P. F. Lagerwall, *Angew. Chem.*, 2020, **132**, 19422 – 19429.
15 M. Tenjimbayashi, S. Samitsu, Y. Watanabe, Y. Nakamura and M. Naito, *Adv. Funct. Mater.*, 2021, **31**, 2010957.
16 Joshua Saczek, Xiaoxue Yao, Vladimir Zivkovic, Mohamed Mamlouk, Dan Wang, Stevin S. Pramana, and Steven Wang, Adv. Funct. Mater. 2021, 31, 2011198.
17 Zhuo Xin and Troels Skrydstrup, Angew. Chem. Int. Ed. 2019, 58, 11952 – 11954.
18 C. Gabbott, E. Mele, T. Sun, *J. Biotechnol.* **2020**, *323*, 82.
19 X. Rong, R. Ettelaie, S. V. Lishchuk, H. Cheng, N. Zhao, F. Xiao, F. Cheng, H. Yang, *Nat. Commun.* **2019**, *10*, 1854.
20 J. Canivet, A. Fateeva, Y. Guo, B. Coasne and D. Farrusseng, *Chem. Soc. Rev.*, 2014, **43**, 5594.
21 Q. Wang and D. Astruc, Chem. Rev., 2020, **120**, 1438−1511.
22 R. Freund, O. Zaremba, G. Arnauts, R. Ameloot, G. Skorupskii, M. Dinca, A. Bavykina, J. Gascon, A. Ejsmont, J. Goscianska, M. Kalmutzki, U. Lächelt, E. Ploetz, C. S. Diercks and S. Wuttke, *Angew. Chem. Int. Ed*., 2021, **60**, 23975–24001.
23 D. Sun, P. R. Adiyala, S.-J. Yim and D.-P. Kim, *Angew. Chem. Int. Ed*., 2019, **58**, 7405–7409.
24 D. M. DeChellis, C. M. Ngule and D. T. Genna, *J. Mater. Chem. A*, 2020, **8**, 5848.
25 L. Feng, S.-H. Lo, K. Tan, S.-L. Wang, K.-L. Lu and H.-C. Zhou, *Matter*, 2020, **2**, 988–999.
26 H. Saini, P. Kallem, A. Schneemann, V. Ranc, M. Otyepka, R. A. Fischer, E. Otyepkova, F. Geyer, F. Banat, R. Zboˇril and K. Jayaramulu, *J. Mater. Chem. A*, 2021, **9**, 23651.
27 Y. Zhang, X. Feng, H. Li, Y. Chen, J. Zhao, S. Wang, L. Wang and B. Wang, *Angew. Chem. Int. Ed*., 2015, **54**, 4259–4263.
28 H. Wang, S. He, X. Qin, C. Li and T. Li, *J. Am. Chem. Soc.*, 2018, **140**, 17203−17210.
29 H. A. Hamzah, T. S. Crickmore, D. Rixson and A. D. Burrows, *Dalton Trans*., 2018, **47**, 14491.
30 S. Wang, C. M. McGuirk, A. d. Aquino, J. A. Mason and C. A. Mirkin, *Adv. Mater.*, 2018, **30**, 1800202.
31 U. Baruah and U. Manna, *Chem. Sci.*, 2021, **12**, 2097.
32 M. Inoue, M. Paven, H. Mayama, H.-J. Butt, Y. Nakamura and S. Fujii, Polym. J. 2011, 43, 778-784.
33 H. Kawashima, S. Fujii, Y. Nakamura, Y. Iwasaki and S.-I. Yusa, ACS Appl. Mater. Interfaces, 2017, 9, 33351−33359.
34 Z. Zhaoa, S. Qina, D. Wanga, Y. Pua, J.-X. Wanga, J. Saczekc, A. Harveyc, C. Lingd, S. Wangd and J-F Chen, *Chem. Eng. J.*, 2020, **391**, 123478.
35 M. Uda, H. Kawashima, H. Mayama, T. Hirai, Y. Nakamura and S. Fujii, Langmuir, 2021, 37, 4172−4182.
36 Z. Zhao, X. Yao, W. Zhao, B. Shi, S. Sridhar, Y. Pu, S. Pramana, D. Wang and S. Wang, Chem. Eng. J., 2022, 443, 136417.
37 Y. Tsumura, K. Oyama, A.-L. Fameau, M. Seike, A. Ohtaka, T. Hirai, Y. Nakamura and S. Fujii, ACS Appl. Mater. Interfaces, 2022, 14, 41618−41628.
38 B. Wang, G.-X. Yan, Y.-J. Cheng, E.-X. Chen, L. He, X. Zhou, Y. Dai, M.-B. Luo and Q. Lin, *Inorg. Chem.* 2023, **62**, 10054−10058.
39 J. C. Gomez, N. S. Vishnosky, S. T. Kim, S. A. Dinca, E. B. Finkelstein and R. C. Steinhardt, *Adv. Funct. Mater.* 2023, **33**, 2214893.
40 N. Barman, A. Shome, S. Kumar, P. Mondal, K. Jain, M. Tenjimbayashi, and U. Manna, *Adv. Funct. Mater.* 2023, **33**, 2214840.
41 N. Vogel, J. Ally, K. Bley, M. Kappl, K. Landfester and C. K. Weiss, Nanoscale, 2014, **6**, 6879.
42 H.-H. Ren, Y. Fan, B. Wang and L.-P. Yu, *J. Agric. Food Chem.*, 2018, **66**, 8851.
43 WHO (World Health Organization), *Guidelines for Drinking water Quality*, WHO, Geneva, 3rd edn, 2004.
44 J. B. Fox, *Anal. Chem.* 1979, **51**, 1493.
45 P. J. Larkin, General Outline for IR and Raman Spectral Interpretation, *Infrared and Raman Spectroscopy: Principles and Spectral Interpretation*, 2nd edn, 2018, p. 135.